Supporting Information

For

Nontarget Screening of Per- and Polyfluoroalkyl Substances Binding to Human Liver Fatty Acid Binding Protein

Diwen Yang[a], Jiajun Han[a], David Ross Hall[a], Jianxian Sun[a], Jesse Fu[a], Steven Kutarna[a], Keith A. Houck[b], Carlie A. LaLone[c], Jon A. Doering[c,d], Carla A. Ng[e], Hui Peng[*a,f]

[a] Department of Chemistry, University of Toronto, Toronto, ON, Canada
[b] Center for Computational Toxicology and Exposure, Office of Research and Development, United States Environmental Protection Agency, Research Triangle Park, NC, 27711 USA
[c] Great Lakes Toxicology and Ecology Division, U.S. Environmental Protection Agency, Duluth, Minnesota 55804 United States
[d] National Research Council, U.S. Environmental Protection Agency, Duluth, Minnesota 55804 USA
[e] Department of Civil & Environmental Engineering, University of Pittsburgh, 3700 O'Hara St, Pittsburgh, USA
[f] School of the Environment, University of Toronto, Toronto, ON, Canada

***Corresponding author: Hui Peng**, e-mail: hui.peng@utoronto.ca, Department of Chemistry, University of Toronto, Toronto, Ontario, M5S3H6, Canada.

Words 2015
Tables 3
Figures 8

This supporting information provides text and figures addressing (1) Chemical and reagents used; (2) Overexpression of *h*L-FABP; (3) Fluorescence displacement assay; (4) Dissociation constants (K_d) of PFASs binding to *h*L-FABP; (5) Sample collection and preparation; (6) Small molecule analysis with LC-Orbitrap; (7) Proteome analysis with liquid chromatography and high-resolution mass spectrometry; (8) Nontarget/suspect data analysis; (9) The chemical number, name and molecular formula and structures of 74 per- and polyfluoroalkyl substances (PFASs); (10) The inhibition concentration, dissociation constants, peak intensity and retention time of 20 *h*L-FABP ligands; (11) Western blot analysis of overexpressed His-tagged *h*L-FABP. (12) Direct binding of 1,8-ANS to *h*L-FABP; (13) Calculation process of dissociation constants (K_d) of PFASs; (14) The dose-response curves of 20 PFASs; (15) Verification of *h*L-FABP in SEC fraction F2 by proteomics; (16) PFOS impurity in NEt-FOSA standards; (17) Confirmation of PFPeS and PFHpS by their authentic standards; (18) Confirmation of the secondary structure of *h*L-FABP via Circular Dichroism (CD) spectrometer.

Chemicals and Reagents. The characterization of the stability of the 74 standard solutions during storage was in progress by EPA. To confirm the identity of 74 PFASs, 74 PFASs were dissolved in methanol to reach the final concentration of 1μM of each PFAS. The PFASs were subjected to LC-Orbitrap for analysis (details are provided below). Stock solutions of 30 mM concentrations of 74 PFASs were prepared in dimethyl sulfoxide (DMSO) and stored at -20 °C. A commercial AFFF technical product was the representative AFFFs used in different Air Force bases in USA. *h*L-FABP pNIC28-Bsa4 plasmid (plasmid #42344) was purchased from Addgene (Cambridge, MA, USA). BL21(DE3) competent *Escherichia coli* was purchased from BioLabs Inc. (Whitby, ON, CA). Isopropyl-β -D-thiogalactopyranoside (IPTG) and 1-anilinonaphthalene-8-sulfonic acid (1,8-ANS) were purchased from Thermo Fisher Scientific (Ottawa, ON, CA). Supelclean™ ENVI™-18 solid-phase extraction (SPE) cartridges (6 mL, 1g) were purchased from Sigma-Aldrich (St. Louis, MO, USA). Trypsin Gold (mass spectrometry grade) was obtained from Promega (Madison, WI, USA). Triethyl ammonium bicarbonate buffer (TEAB), tris(2-carboxyethyl)phosphine hydrochloride (TCEP), iodoacetamide, cOmplete Mini EDTA-free protease inhibitor cocktail tablets, and dithiothreitol (DTT) were obtained from Sigma-Aldrich (St. Louis, MO, USA). Phosphate-Buffered Saline tablets, HEPES and tris-HCL were purchased from BioShop Canada Inc. (Burlington, ON, Canada). Ultrapure water, methanol and acetonitrile (HPLC grade) were purchased from Fisher Scientific (Ottawa, ON, CA). Formic acid (mass spectrometry grade) was purchased from EMO Millipore (St. Louis, MO, USA).

Overexpression of *h*L-FABP. *h*L-FABP pNIC28-Bsa4 plasmid (plasmid #42344) was purchased from Addgene (Cambridge, MA, USA). The plasmid was transformed into BL21 (DE3) strain of *Escherichia coli*. The *h*L-FABP protein was overexpressed by adding in 1 mM IPTG followed by overnight incubation at 18 °C. Bacterial cells were lysed by sonication in a lysis buffer (10 mM

HEPES, 100 mM NaCl, 0.2 mM EDTA, 10% glycerol, 0.5 mM DTT and protease inhibitors cocktail (Sigma S8830, pH 7.4)) as described previously.[1] The total protein concentration was measured by the Bradford protein assay. The identity of *h*L-FABP was confirmed by SDS-PAGE and western blot with an anti-His antibody (Figure S1).

Circular Dichroism (CD) Spectroscopy. Recombinant his-tagged *h*L-FABP were loaded into a circular cuvette with a 1mm pathlength and analyzed on a Jasco J-710 circular dichroism spectrophotometer at room temperature. Spectra was acquired from 800nm to 190 nm with 2 nm resolution, with baseline subtraction of the background PBS buffer. Reference L-FABP CD spectrum downloaded from the *Protein Circular Dichroism Databank* [2](reference number CD0004134000). We also used the *PDB2CD* web-application[3] to predict *h*L-FABP CD spectrum from structural data produced by Patil et al.[4] (PDB entry 6DO6) and the SP175 soluble proteins reference database. The CD spectra of purified his-tagged *h*L-FABP is consistent with reference and predicted spectrum (Figure S8), and also the experimental spectra determined in a previous study.[5] These results demonstrated that the *h*L-FABP protein structure was well preserved during the experiments.

Fluorescence Displacement Assay. The binding of 74 PFASs to *h*L-FABP was individually determined by the displacement of bound 1,8-ANS from *h*L-FABP as previously described.[6] To initially determine the interactions between 74 PFASs and *h*L-FABP, we investigated the fluorescence displacement of 1,8-ANS by PFASs at a fixed concentration of 300 μM. In brief,1 μL of 4 mM 1,8-ANS was added in 100 μL buffer A (50 mM tri-HCL, 150 mM NaCl, 1 mM dithiothreitol, pH 8.0) with *h*L-FABP (1 μM). Following incubation at room temperature for 30 min, 1 μL of the stock solution of each PFASs (final concentration = 300 μM) was added in fluorescence probe solution (*n = 3*) individually. The mixtures were incubated for 30 min at room

temperature. The fluorescence signal was measured via an Infinite 200 PRO multimode plate reader (Tecan Group Ltd., Switzerland) with 350 nm excitation wavelength and emission spectra between 420 nm and 600 nm. The 30 PFASs causing > 10% reduction of fluorescence intensity were considered as potential *h*L-FABP ligands and thus selected for K_d measurement.

Dissociation Constants (K_d) of PFASs Binding to *h*L-FABP. The dissociation constant (K_{dA}) of 1,8-ANS was experimentally derived from the measurement of maximal fluorescence intensities of bound 1,8-ANS at various concentrations (0-50 μM, *n = 3*) (Figure S2). The one-site binding model based Scatchard equation (eq 1) was fit to the displacement of protein-bound 1,8-ANS to calculate K_{dA}:

$$\frac{[L_{ANS}]_f}{r} = \frac{[L_{ANS}]_f}{n} + \frac{K_{dA}}{n} \quad (1)$$

where $[L_{ANS}]_f$ represents the concentrations of free 1,8-ANS; K_{dA} represents the dissociation constant of 1,8-ANS; n represents the number of binding sites which is 1 for 1,8-ANS and *h*L-FABP; r is the number of moles of bound 1,8-ANS per mole of *h*L-FABP which is fixed to 1. With the Scatchard equation, the K_{dA} was calculated to be 18.0 μM, similar to the results reported in a previous study.[7]

With K_{dA} values, the dissociation constants (K_d) of PFASs were determined from the displacement of protein-bound 1,8-ANS by PFASs at different concentrations (*n = 3*). Specifically, concentrations of 1.23, 3.7, 11.1, 33.3, 100, 300 μM were selected for high-affinity PFASs, while only high concentrations (50, 75, 150, 300 μM) were used for low-affinity PFASs. In brief, 1 μL of stock solution of each 74 PFASs was individually added into a 100 μL mixture of *h*L-FABP (1 μM) and 1,8-ANS (40 μM) in buffer A which had been incubated for 30 min to reach equilibrium before adding PFAS. The measurement of fluorescence intensity was done after 30 min incubation at room temperature. The displacement of 1,8-ANS binding to *h*L-FABP by increasing

concentrations of PFAS was corresponding to a reduction in fluorescence intensity. K_d values of PFASs were determined by fitting to a sigmoidal model (Figure S3, SI). The GraphPad Prism V7.0 was used to plot dose-response curves in which the IC_{50} value of 9 PFASs or IC_{10} value of 11 PFASs were derived.

With the $IC_{50/10}$ of each PFASs, the corresponding K_d values were obtained through the Cheng-Prusoff equation[8]:

$$f_{PFAS} = \frac{[L_{ANS}]}{K_{dA}\left(1 + \frac{[L_{PFAS}]}{K_d}\right) + [L_{ANS}]} \quad (2)$$

where f_{PFAS} represents fractional occupancy of PFAS binding to *h*L-FABP by displacing 1,8-ANS; L_{PFAS} represents the concentration of PFAS; K_d represents dissociation constant of PFAS.

Therefore, for high-affinity ligands when IC_{50} could be reliably determined, K_d values were calculated by rearranging eq 2 to eq 3:

$$K_d = \frac{IC_{50}}{1 + \frac{[L_{ANS}]}{K_{dA}}} \quad (3)$$

Similarly, for low-affinity PFASs for which only IC_{10} is determined, K_d values were calculated by rewriting eq 2 to eq 4:

$$K_d = \frac{9 \times IC_{10}}{1 + \frac{[L_{ANS}]}{K_{dA}}} \quad (4)$$

Sample Collection and Preparation. Water samples were collected from the west end of Lake Niapenco which was reported to be contaminated by AFFF chemicals from John C. Munro International Airport, Hamilton, ON. Water samples were collected using polypropylene tubes which were then stored on ice during the transportation and extracted within 10 hours. Water samples were centrifuged at 4000 g for 10 min at 4 °C. Following centrifugation, 100 mL of water samples were extracted with solid-phase extraction (SPE) cartridges (Supelclean™ ENVI™-18 SPE, 6 mL, 1g), a common SPE previously used for nontarget analysis.[9] The SPE cartridges were

preconditioned with 6 mL of methanol and equilibrated with 6 mL of ultra-pure water. Water samples were then passed through the conditioned SPE cartridges at a flow rate of 1–2 drops/s. AFFF chemicals were eluted with 5 mL of methanol. The eluents were reconstituted in 50 μL of methanol after dryness under nitrogen flow. A procedural blank was incorporated by loading 100 mL of ultrapure water onto the SPE cartridges with the same procedure, and no background contamination was detected.

Small Molecule Analysis with LC-Orbitrap. PFASs analysis including NTA analysis was conducted using a Q Exactive mass spectrometry equipped with a Vanquish UHPLC system (Thermo Fisher Scientific, USA). Separation of PFASs and AFFF chemicals was achieved with Accucore Vanquish C18 column (50 × 2.1 mm, 1.5 μm, Thermo Scientific). The Injection volume was 2 μL with 1% formic acid in ultrapure water (A) and 1% formic acid in acetonitrile (B) as mobile phases. Initially, 10% B was increased to 80% in 2 min, then increased to 100% at 5 min and held static for 3 min, followed by a decrease to initial conditions of 10% B and held for 1min to allow for equilibration. The flow rate was 0.15 mL/min. The column and sample compartment temperatures were maintained at 40 °C and 4 °C, respectively. For the analysis of 74 PFASs, data were acquired in full MS mode. Parameters for full scan (100–1000 *m/z*) switch mode recorded at resolution R = 70 000 (at *m/z* 200) with a maximum of 3×10^6 ions collected within 200 ms. For NTA of AFFF chemicals, data were acquired in data-independent acquisition (DIA) mode. Parameters for full MS scan Parameters for DIA were one full MS^1 scan (100–1000 *m/z*) recorded at resolution R = 70 000 (at *m/z* 200) with a maximum of 3×10^6 ions collected within 100 ms, followed by DIA MS/MS scan (200–500 *m/z*) recorded at resolution R = 35 000 (at *m/z* 200) with a maximum of 1×10^5 ions collected within 60 ms. DIA data were collected by use of 10 *m/z* isolation windows per MS/MS scan, in total, there were 30, 10-*m/z* wide windows between 200–500 *m/z*. Mass spectrometric settings for ESI (-) mode which were the used for both full MS

mode and DIA mode were as follows: spray voltage, 2.7 kV; sheath gas flow rate, 30 L/h; auxiliary gas flow rate, 6 L/h; capillary temperature 300 °C.

Proteome Analysis with Liquid Chromatography and High-Resolution Mass Spectrometry. For proteome analysis, the proteins from each SEC fraction were precipitated with 4-fold volumes of cold acetone at -20 ^{o}C followed by re-dissolving in 1M TEAB. The protein samples were then reduced with 5 mM tris(2-carboxyethyl)phosphine hydrochloride (TCEP) for 60 min, carboxymethylated with 15 mM iodoacetamide in the dark at room temperature for 30 min. The proteins were then digested with trypsin (4 μg) for 16 hours at 37 ^{o}C. Digestion was terminated by adding formic acid to 1% (v/v). The tryptic peptides were analyzed by Q Exactive Quadrupole-Orbitrap Mass Spectrometer (Thermo Fisher Scientific, USA) coupled with a Vanquish UHPLC system (Thermo Fisher Scientific, USA).[1] 3 μL of each sample were loaded on Acclaim PepMap 100 C18 LC Columns (75μm × 2cm, nanoViper, 3μm, 100Å, Thermo Fisher Scientific, USA) for analytical separations of peptides. (A) 1% formic acid in acetonitrile (v/v) (B) 1% formic acid in ultrapure water (v/v) were used as mobile phases at a 0.120 mL/min flow rate. Initially, B was increased from 5% to 50% in 6 mins, then increased to 100% in 12 mins, and kept static for 1 min following by a decrease to initial conditions of 5% B and held for 1 min to allow for equilibration, the total method duration was 15 min. The positively charged ions were subjected to 400-1500 *m/z* full scan with 70,000 resolution, 60 ms maximum IT and 3×10^6 AGC target. The secondary mass spectrometry data were acquired under data-dependent single ion monitor mode (dd-SIM) with 17,500 resolution, 50 ms maximum IT, 2.0 isolation window, 2×10^5 AGC target, 4×10^4 intensity threshold and 10s dynamic exclusion.

Nontarget/Suspect Data Analysis. Nontarget data analysis was accomplished with an in-house R program. Raw mass spectrometry files were converted to mzXML format. The peaks were

detected with the XCMS package at a mass tolerance of 2.5 ppm.[10] The peak features were matched across samples with a mass tolerance of 2.5 ppm and retention time window of 20 seconds, after retention time adjustment. The ratio of abundances in F2 from *h*L-FABP lysates to those in F2 from wild type *E. coli* lysates, was calculated for each peak feature. The *p*-value of the difference between the two groups was also determined by student's t-test. Only the features exhibiting greater peak intensities (fold change > 10, *p*-value < 0.05) in extracts from *h*L-FABP overexpressing lysates were considered as potential *h*L-FABP ligands. Isotopic peaks and adducts were excluded by matching chromatographic peaks and theoretical mass difference. The final differentiated peak list from the output of the R program was manually checked using MS^1 mass and retention time.

The features were searched against PFAS (1,021 PFASs) and AFFF surfactant (869 surfactants) libraries established in two recent studies,[11, 12] with a mass tolerance of 3 ppm. Confidence levels were assigned to all identities according to the Schymanski et al. scale.[13] In brief, a level 1 confidence was assigned to PFASs for which authentic standards are available for confirmation by matching retention time, MS^1 and MS^2. In the case of AFFF surfactants, the confidence levels fall to levels 2 or 3, in which molecular ions and fragmentation were matched. For instance, SO_3^- and HSO_4^- were detected as diagnostic fragments of alkyl ether sulfates.

Table S1: The summary of 74 per- and polyfluoroalkyl substances (PFASs) from U. S. Environmental Protection Agency (EPA) PFAS screening library[48] with chemical number, name, molecular formula and structure. The PFASs have been categorized based on their chemical structures. The chemical number is consistent with the U.S.EPA PFAS screening library.

Category	No	CASRN	Name	Molecular Formula	Structure
Alcohols	41	2043-47-2	4:2 Fluorotelomer alcohol	$C_6H_5F_9O$	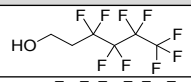
	70	647-42-7	6:2 Fluorotelomer alcohol	$C_8H_5F_{13}O$	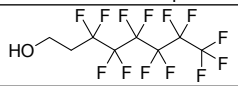
	64	678-39-7	8:2 Fluorotelomer alcohol	$C_{10}H_5F_{17}O$	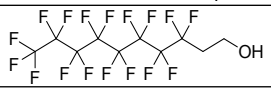
	11	375-01-9	Heptafluorobutanol	$C_4H_3F_7O$	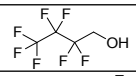
	48	355-80-6	1H,1H,5H-Perfluoropentanol	$C_5H_4F_8O$	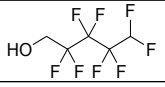
	67	335-99-9	Dodecafluoroheptanol	$C_7H_4F_{12}O$	
	50	423-65-4	11:1 Fluorotelomer alcohol	$C_{12}H_3F_{23}O$	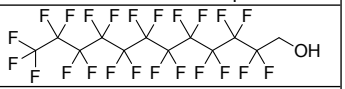
	49	679-02-7	3-(Perfluoropropyl)propanol	$C_6H_7F_7O$	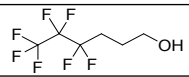
	40	3792-02-7	4:4 Fluorotelomer alcohol	$C_8H_9F_9O$	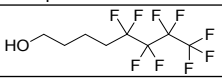
	61	1694-30-0	3H-Perfluoro-4-hydroxy-3-penten-2-one	$C_5H_2F_6O_2$	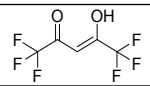
	32	129301-42-4	1H,1H,8H,8H-Perfluoro-3,6-dioxaoctane-1,8-diol	$C_6H_6F_8O_4$	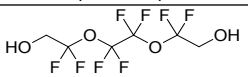
	62	374-40-3	1-Pentafluoroethylethanol	$C_4H_5F_5O$	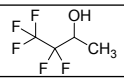
	30	125070-38-4	3-(Perfluoro-2-butyl)propane-1,2-diol	$C_7H_7F_9O_2$	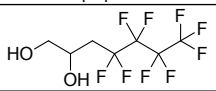
	35	376-90-9	Hexafluoroamylene glycol	$C_5H_6F_6O_2$	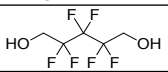
	66	77953-71-0	3H-Perfluoro-2,2,4,4-tetrahydroxypentane	$C_5H_5F_7O_4$	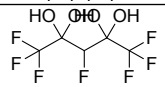
Carboxylates	4	679-12-9	4H-Perfluorobutanoic acid	$C_4H_2F_6O_2$	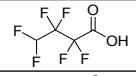
	12	375-22-4	Perfluorobutanoic acid	$C_4HF_7O_2$	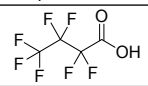
	14	914637-49-3	2H,2H,3H,3H-Perfluorooctanoic acid	$C_8H_5F_{11}O_2$	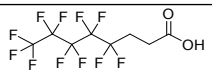
	17	375-95-1	Perfluorononanoic acid	$C_9HF_{17}O_2$	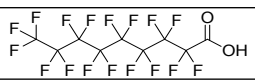

	20	307-24-4	Perfluorohexanoic acid	$C_6HF_{11}O_2$	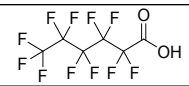
	21	3825-26-1	Ammonium perfluorooctanoate	$C_8H_4F_{15}NO_2$	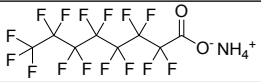
	74	335-67-1	Perfluorooctanoic acid	$C_8HF_{15}O_2$	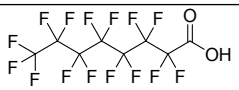
	23	1763-28-6	3,3-Bis(trifluoromethyl)-2-propenoic acid	$C_5H_2F_6O_2$	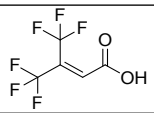
	56	243139-64-2	3-(Perfluoroisopropyl)-2-propenoic acid	$C_6H_3F_7O_2$	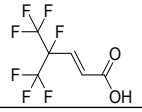
Sulfonates	6	2795-39-3	Potassium perfluorooctanesulfonate	$C_8F_{17}KO_3S$	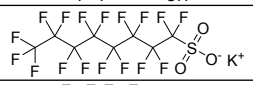
	15	757124-72-4	4:2 Fluorotelomer sulfonic acid	$C_6H_5F_9O_3S$	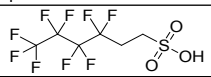
	26	3871-99-6	Potassium perfluorohexanesulfonate	$C_6F_{13}KO_3S$	
	46	1763-23-1	Perfluorooctanesulfonic acid	$C_8HF_{17}O_3S$	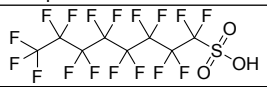
	57	29420-49-3	Potassium perfluorobutanesulfonate	$C_4F_9KO_3S$	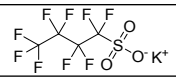
	73	375-73-5	Perfluorobutanesulfonic acid	$C_4HF_9O_3S$	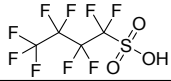
Amides	5	1652-63-7	Perfluorooctanesulfonamido ammonium iodide	$C_{14}H_{16}F_{17}N_2O_2S$	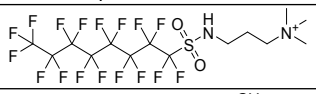
	9	1691-99-2	N-Ethyl-N-(2-hydroxyethyl)perfluorooctanesulfonamide	$C_{12}H_{10}F_{17}NO_3S$	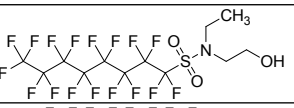
	16	31506-32-8	N-Methylperfluorooctanesulfonamide	$C_9H_4F_{17}NO_2S$	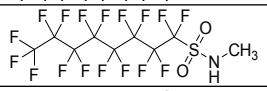
	19	13485-61-5	Nonafluoropentanamide	$C_5H_2F_9NO$	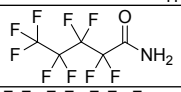
	24	4151-50-2	N-Ethylperfluorooctanesulfonamide	$C_{10}H_6F_{17}NO_2S$	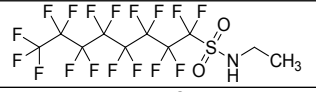
	31	662-50-0	Heptafluorobutyramide	$C_4H_2F_7NO$	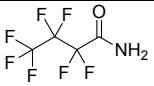
	38	355-81-7	Perfluoropentanamide	$C_5H_3F_8NO$	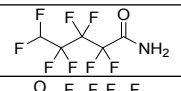
	58	355-66-8	Octafluoroadipamide	$C_6H_4F_8N_2O_2$	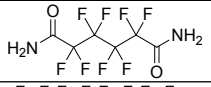
	60	754-91-6	Perfluorooctanesulfonamide	$C_8H_2F_{17}NO_2S$	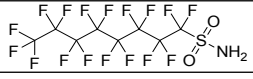

	68	355-27-1	1H,1H-Perfluoropentylamine	$C_5H_4F_9N$	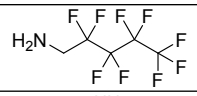
	71	1619-92-7	2-Amino-2H-perfluoropropane	$C_3H_3F_6N$	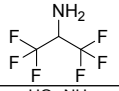
	33	31253-34-6	2-Aminohexafluoropropan-2-ol	$C_3H_3F_6NO$	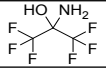
	45	883498-76-8	Bis(1H,1H-perfluoropropyl)amine	$C_6H_5F_{10}N$	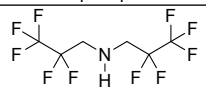
Ethers	34	330562-41-9	Perfluoro-3,6,9-trioxatridecanoic acid	$C_{10}HF_{19}O_5$	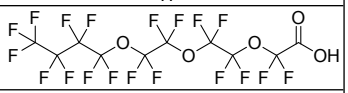
	7	55621-21-1	Perfluoro-3,6-dioxaoctane-1,8-dioic acid	$C_6H_2F_8O_6$	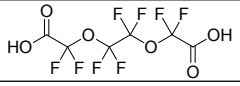
	2	2144-53-8	6:2 Fluorotelomer methacrylate	$C_{12}H_9F_{13}O_2$	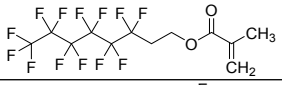
	10	329710-76-1	2-(Trifluoromethoxy)ethyl trifluoromethanesulfonate	$C_4H_4F_6O_4S$	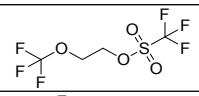
	13	74427-22-8	2,2-Difluoroethyl triflate	$C_3H_3F_5O_3S$	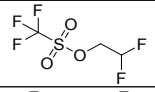
	27	333-36-8	Flurothyl	$C_4H_4F_6O$	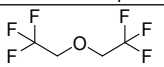
	28	863090-89-5	Perfluoro(4-methoxybutanoic) acid	$C_5HF_9O_3$	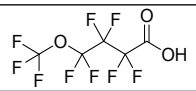
	37	13252-13-6	Perfluoro-2-methyl-3-oxahexanoic acid	$C_6HF_{11}O_3$	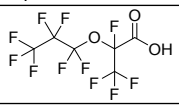
	1	58244-27-2	Tris(Trifluoroethoxy)methane	$C_7H_7F_9O_3$	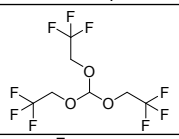
	18	15242-17-8	Allyl perfluoroisopropyl ether	$C_6H_5F_7O$	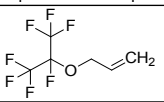
	44	163702-08-7	Perfluoroisobutyl methyl ether	$C_5H_3F_9O$	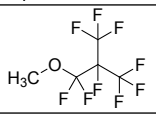
	3	28523-86-6	Sevoflurane	$C_4H_3F_7O$	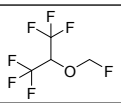
	52	56860-81-2	Difluoromethyl 1H,1H-perfluoropropyl	$C_4H_3F_7O$	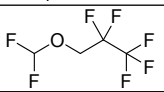
	53	1623-05-8	Heptafluoropropyl trifluorovinyl ether	$C_5F_{10}O$	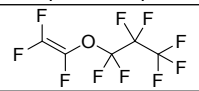
	54	151772-58-6	Perfluoro-3,6-dioxaheptanoic acid	$C_5HF_9O_4$	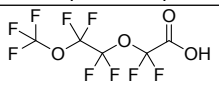

	65	163702-05-4	Ethyl perfluorobutyl ether	$C_6H_5F_9O$	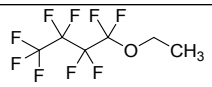
Acetates	47	356-24-1	Methyl heptafluorobutyrate	$C_5H_3F_7O_2$	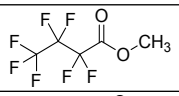
	36	424-18-0	Methyl perfluorohexanoate	$C_7H_3F_{11}O_2$	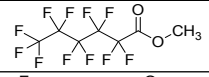
	39	132424-36-3	Methyl 2H,2H,3H,3H-perfluoroheptanoate	$C_8H_7F_9O_2$	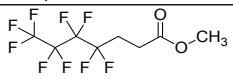
Others	22	355-95-3	1-Propenylperfluoropropane	$C_6H_5F_7$	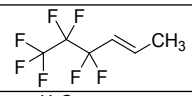
	25	239795-57-4	2-Vinylperfluorobutane	$C_6H_3F_9$	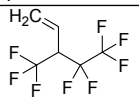
	72	2648-47-7	5H-Perfluoropentanal	$C_5H_2F_8O$	
	42	375-02-0	Perfluorobutyraldehyde	C_4HF_7O	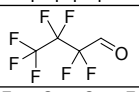
	43	356-42-3	Pentafluoropropanoic anhydride	$C_6F_{10}O_3$	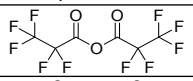
	63	678-78-4	Perfluoroglutaryl difluoride	$C_5F_8O_2$	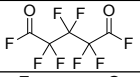
	51	813-03-6	5H-Octafluoropentanoyl fluoride	C_5HF_9O	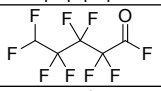
	55	374-41-4	Methyl perfluoroethyl ketone	$C_4H_3F_5O$	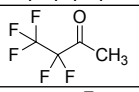
	29	406-58-6	1,1,1,3,3-Pentafluorobutane	$C_4H_5F_5$	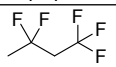
	59	19430-93-4	1H,1H,2H-Perfluoro-1-hexene	$C_6H_3F_9$	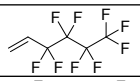
	69	1767-94-8	6H-Perfluorohex-1-ene	C_6HF_{11}	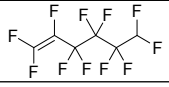

Table S2: The inhibition concentration ($\mathbf{IC_{50/10}}$), dissociation constants ($\mathbf{K_d}$), LC-MS peak intensities (concentration at 1 μM) and retention times of 19 PFASs binding to *h*L-FABP. Results for the other 55 inactive PFASs are not shown. NMe-FOSA (**16**) is excluded from the table since its K_d is greater than 1000 μM even though its peak intensity is very high.

No	IC_{50} (μM)	IC_{10} (μM)	K_d (μM)	Peak Intensity	Retention time (min)
17	13.88	NA	4.30	2.54E+08	4.16
60	18.92	NA	5.87	3.85E+08	4.81
6	26.12	NA	8.10	5.25E+08	4.58
46	26.12	NA	8.10	5.25E+08	4.58
34	26.49	NA	8.22	2.88E+08	4.87
26	36.06	NA	11.19	3.96E+08	3.97
24	53.46	NA	16.58	2.14E+08	5.52
21	60.39	NA	18.74	3.76E+08	3.84
74	60.39	NA	18.74	3.76E+08	3.84
73	NA	41.69	116.40	3.74E+08	3.29
57	NA	44.86	125.25	3.74E+08	3.29
61	NA	48.44	135.24	1.67E+07	2.39
20	NA	50.42	140.76	7.43E+07	3.22
14	NA	56.60	158.03	9.54E+07	4.26
54	NA	90.37	252.31	3.64E+06	3.16
4	NA	125.90	351.53	2.72E+07	1.23
52	NA	256.14	715.15	7.36E+05	3.09
28	NA	291.88	814.93	4.31E+07	2.99
48	NA	328.10	916.06	6.70E+06	3.12

Table S3. Exact masses, retention times, predicted formulas and structures of 11 PFASs in AFFF technical products binding to *h*L-FABP, identified by the SECC method.

m/z	RT (min)	Formula	Structures
348.9377	3.37	$C_5F_{11}SO_3^-$	
398.9342	3.63	$C_6F_{13}SO_3^-$	
498.9275	4.26	$C_8F_{17}SO_3^-$	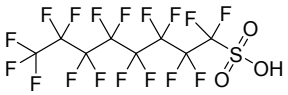
448.9305	3.91	$C_7F_{15}SO_3^-$	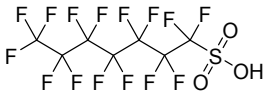
460.9306	3.94	$C_8F_{15}SO_3^-$	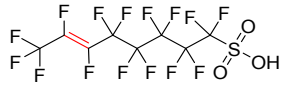
442.9399	3.83	$C_8HF_{14}SO_3^-$	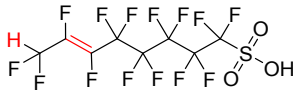
480.9367	4.05	$C_8HF_{16}SO_3^-$	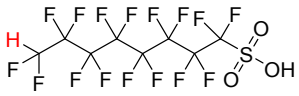
476.9252	4.02	$C_8F_{15}SO_4^-$	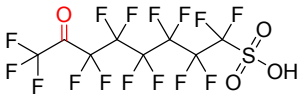
382.9392	3.36	$C_6F_{13}SO_2^-$	
548.9233	4.53	$C_9F_{19}SO_3^-$	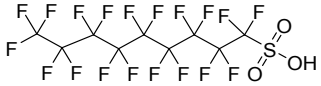
514.8972	4.29	$C_8ClF_{16}SO_3^-$	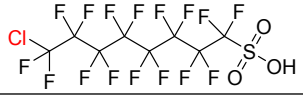

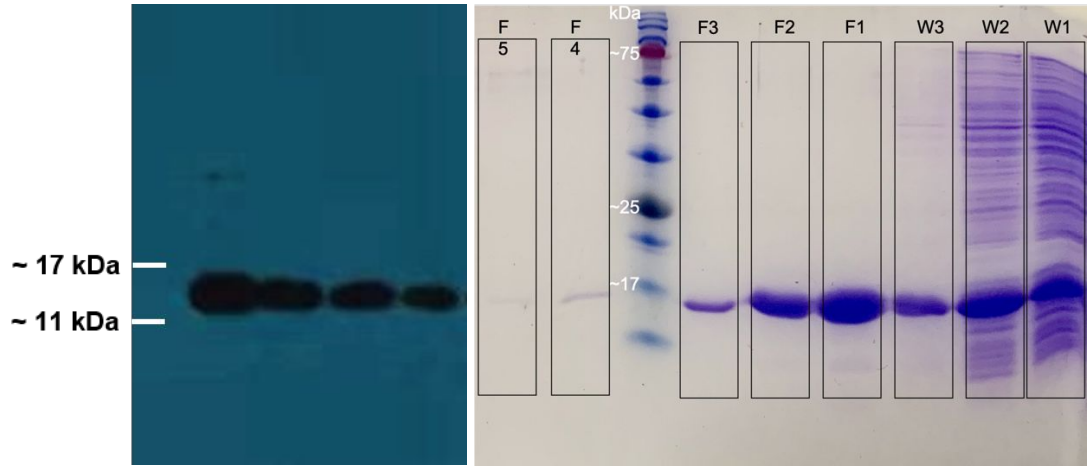

Figure S1: Western blot and SDS-PAGE results of His-tagged *h*L-FABP. (Left) Overexpression of His-tagged *h*L-FABP in *Escherichia coli* from four biological replicates, detected by western blot with His-tag antibody. The molecular weight of *h*L-FABP is around 15 kDa. (Right) SDS-PAGE of purified His-tagged *h*L-FABP where F1 was used for experiments. W1-3 are proteins in the fractions of washing buffer. F1-5 are His-tagged *h*L-FABP in the fraction of elution buffer.

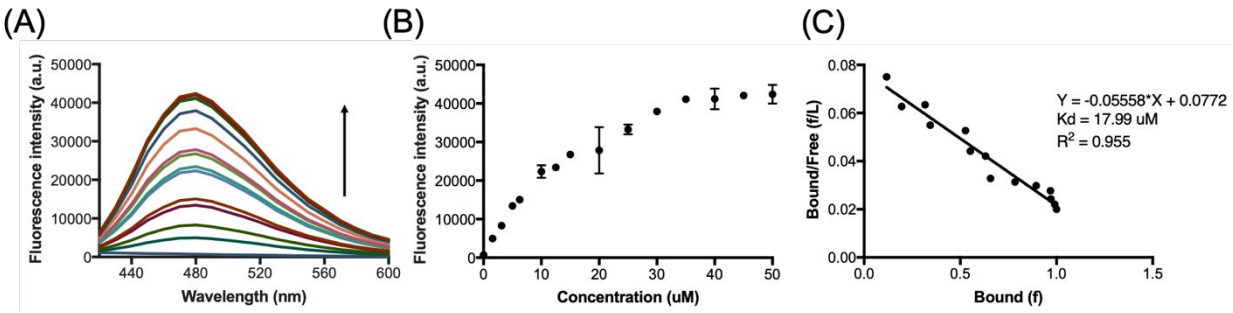

Figure S2: Direct binding of 1,8-ANS to *h*L-FABP. (A) fluorescence emission signal with increasing concentrations of 1,8-ANS in *h*L-FABP. Arrow indicates increasing concentration of 1,8-ANS (0, 1.56, 3.12, 5, 6.25, 10, 12.5, 15, 20, 25, 30, 35, 40, 45, 50 μM). (B) Plot of maximal emission measured at 480 nm for 1,8-ANS in the presence of 1 μM *h*L-FABP as a function of 1,8-ANS concentration. Values are mean ± SE, *n* = *3*. (C) The scratcher plot of 1,8-ANS binding to *h*L-FABP.

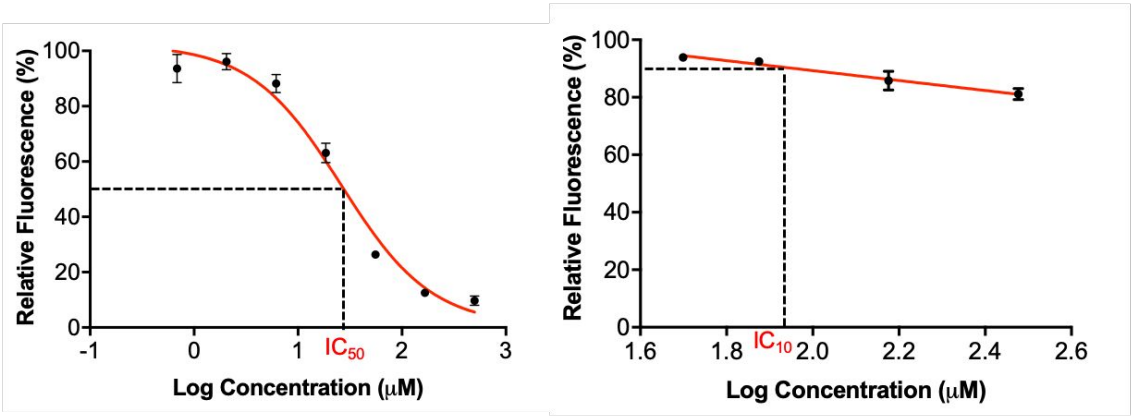

$$P_{FABP} + L_{ANS} \overset{K_{dA}}{\leftrightharpoons} PL \quad (1)$$

$$P_{FABP} + I_{PAFS} \overset{K_d}{\leftrightharpoons} PI \quad (2)$$

$$f_{ANS} = \frac{[L_{ANS}]}{K_{dA} + [L_{ANS}]} \quad (3)$$

$$f_{PFAS} = \frac{[L_{ANS}]}{K_{dA}(1+\frac{[I_{PFAS}]}{K_d}) + [L_{ANS}]} \quad (4)$$

$$IC_{50}: \quad f_{PFAS} = \frac{1}{2} f_{ANS} \quad (5)$$

$$\frac{[L_{ANS}]}{K_{dA}(1+\frac{IC_{50}}{K_d}) + [L_{ANS}]} = \frac{1}{2}\frac{[L_{ANS}]}{K_{dA} + [L_{ANS}]} \quad (6)$$

$$K_d = \frac{IC_{50}}{1 + \frac{[L_{ANS}]}{K_{dA}}} \quad (7)$$

$$IC_{10}: \quad f_{PFAS} = \frac{9}{10} f_{ANS} \quad (8)$$

$$\frac{[L_{ANS}]}{K_{dA}(1+\frac{IC_{10}}{K_d}) + [L_{ANS}]} = \frac{9}{10}\frac{[L_{ANS}]}{K_{dA} + [L_{ANS}]} \quad (9)$$

$$K_d = \frac{9\ IC_{10}}{1 + \frac{[L_{ANS}]}{K_{dA}}} \quad (10)$$

Figure S3: Calculation process of dissociation constants (K_d) of PFASs via dose-response curves obtained by fluorescence displacement assay. (A) Dose-response curve of PFOS (**46**) with calculated IC_{50}. (B) Dose-response curve of perfluoro-3,6-dioxaheptanoic acid (**54**) with calculated IC_{10}. (C) Calculation equations of K_d of PFASs.

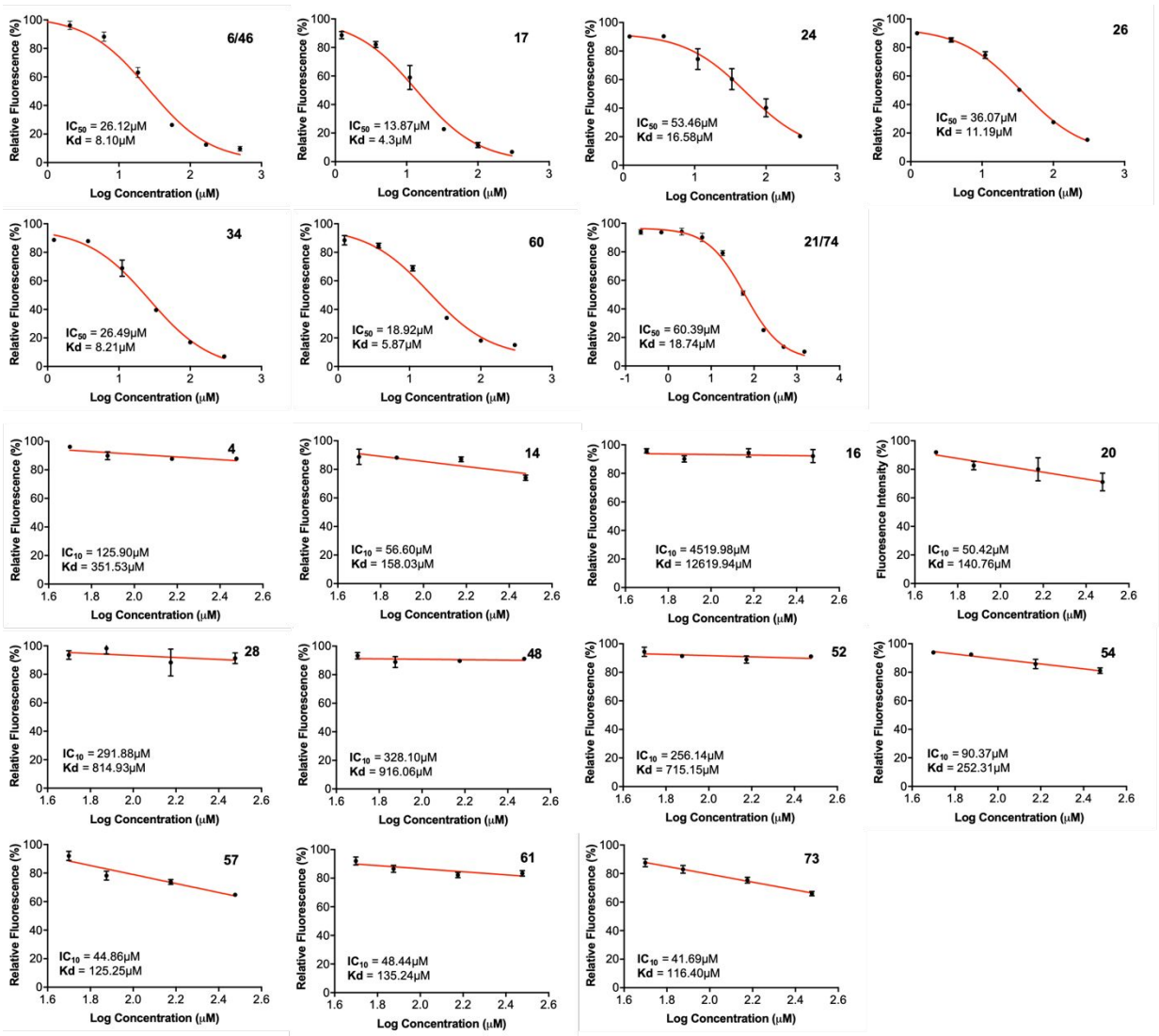

Figure S4: The dose-response curves of 20 PFASs obtained by fluorescence displacement assay with calculated inhibitory concentration ($IC_{50/10}$) and dissociation constant (K_d).

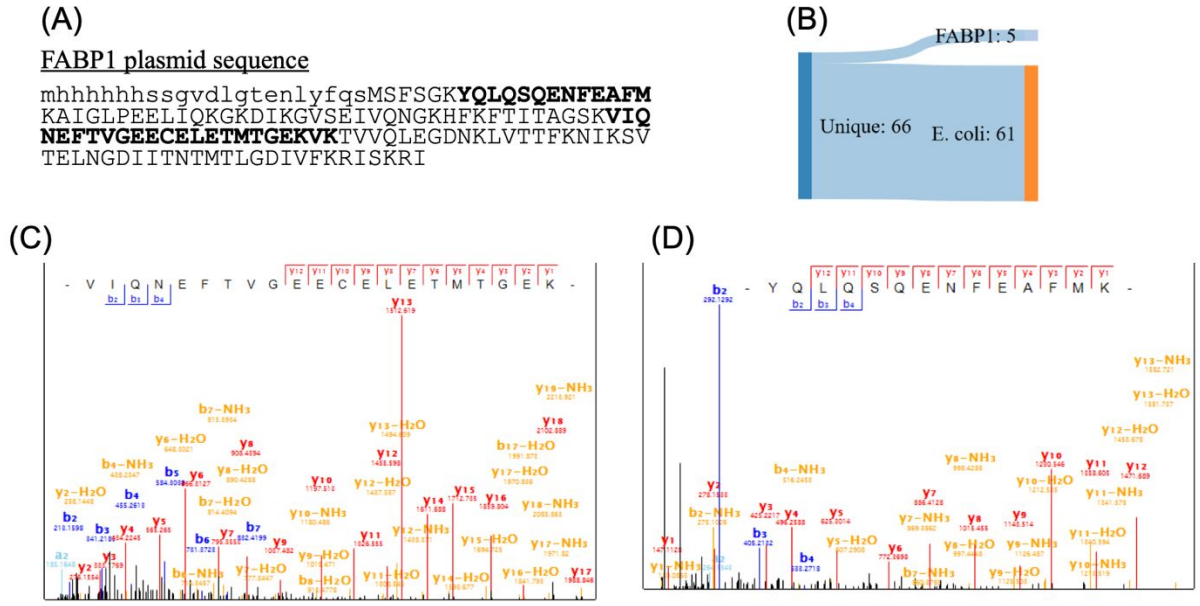

Figure S5: Verification of *h*L-FABP in SEC fraction F2 by proteomics. (a) Amino acid sequence of *h*L-FABP Adgene plasmid #42344 with N-terminal hexahistidine tag (lower case); AA in bold are those sequenced in (C) and (D). (B) Proteomic samples were searched against the *h*L-FABP sequence and the *E. coli* K-12 reference proteome (Uniprot #UP000000625). Of the 73 unique peptides detected in all replicates (n = 3), 5 were assigned to *h*L-FABP. (C, D) Representative MS/MS sequence of two unique *h*L-FABP peptides that were detected in all three replicates.

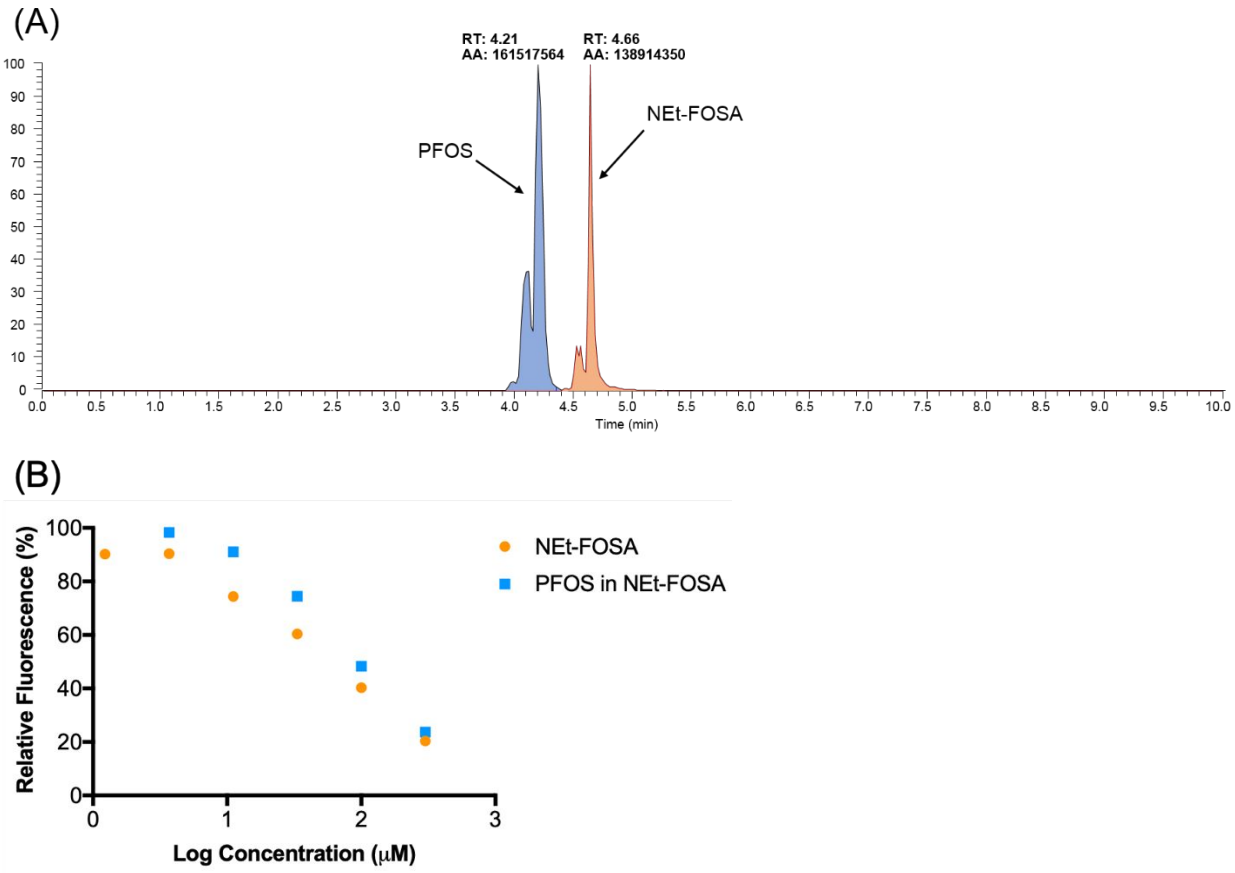

Figure S6: PFOS impurity in NEt-FOSA standard contributes to the activity measured by fluorescence displacement method. (A) LC-MS results of 0.5 μM of NEt-FOSA (orange) standards with a high concentration of PFOS (blue) detected in standards. (B) Relative fluorescence intensity of 40 μM 1,8-ANS in 1 μM *h*L-FABP as a function of adding NEt-FOSA (1.23, 3.7 11.11, 33.33, 100, 300 μM). Blue dots indicate the relative fluorescence percentage as a function of adding NEt-FOSA (**24**), orange dots indicate the estimated relative fluorescence percentage as a function of the impurity PFOS in NEt-FOSA (**24**) obtained through calculation.

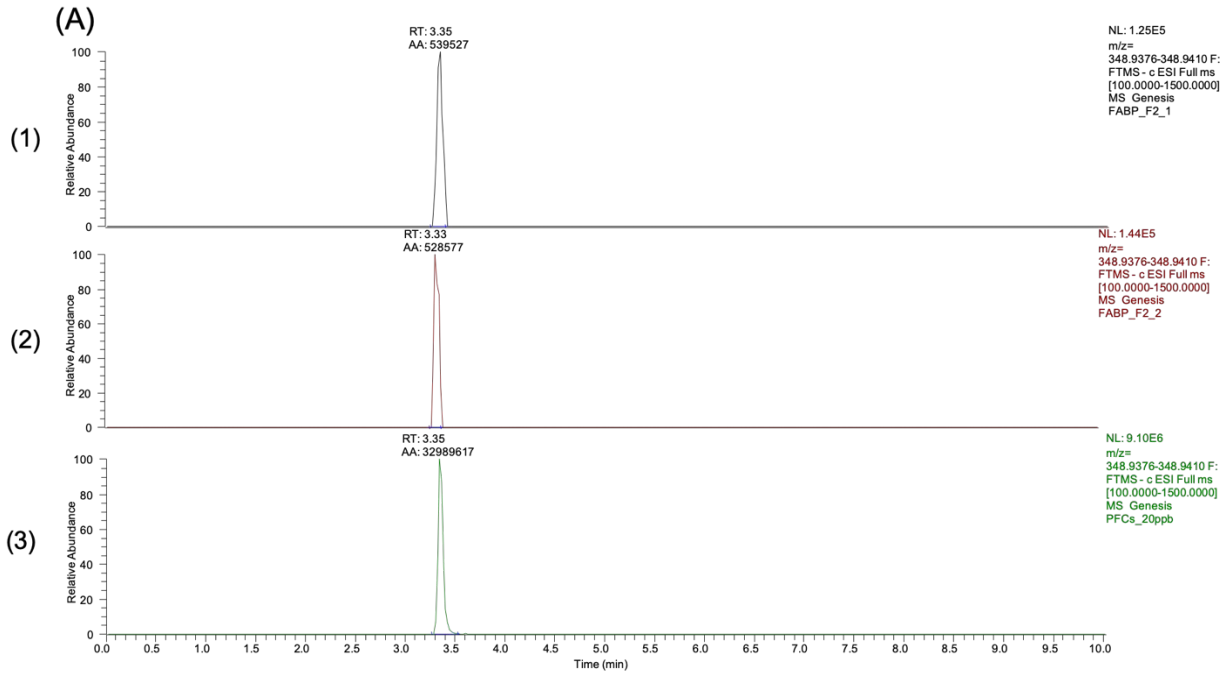

247

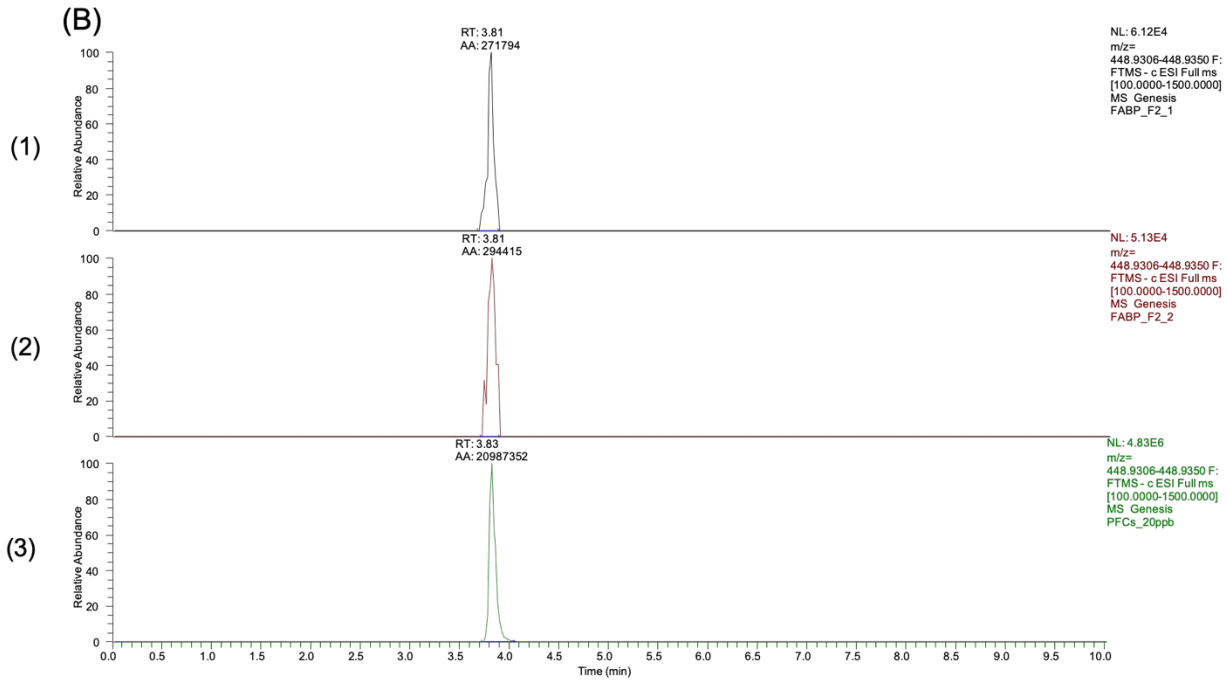

248

249 **Figure S7**: The identities of PFPeS (A), PFHpS (B) in F2 of *h*L-FABP (1, 2 from two replicates)
250 were confirmed by their authentic standards (3).

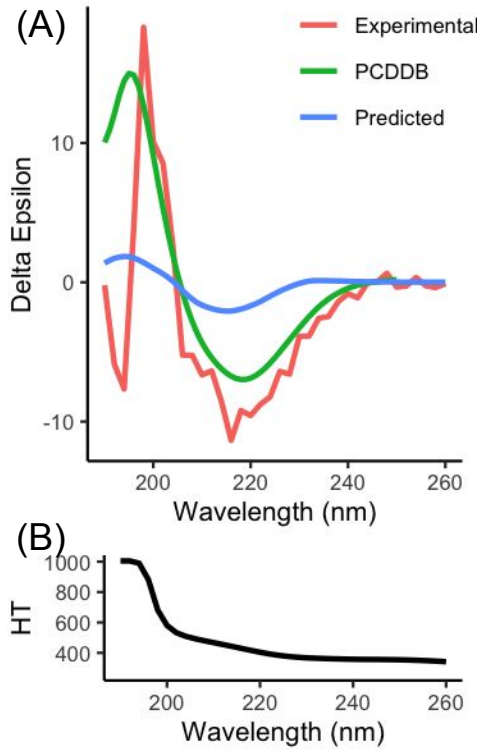

Figure S8: **(A)** Circular Dichroism (CD) spectra of the recombinant poly-his tagged *h*L-FABP protein in *E. coli* used in this study plotted against reference FABP CD spectra (PCDDB) and computational predicted spectra (Predicted); see Experimental Details for additional information. Differences in peak heights result from differences in sample concentration. **(B)** High-tension voltage (HT) of the experimental CD spectrum, the sharp increase around 190 nm accounts for the corresponding sharp decrease in the experimental CD spectra.

References

1. Peng, H.; Saunders, D. M. V.; Sun, J. X.; Jones, P. D.; Wong, C. K. C.; Liu, H. L.; Giesy, J. P. Mutagenic azo dyes, rather than flame retardants, are the predominant brominated compounds in house dust. *Environ. Sci. Technol.* **2016,** *50* (23), 12669-12677.
2. Whitmore, L.; Miles, A. J.; Mavridis, L.; Janes, R. W.; Wallace, B. A. PCDDB: new developments at the Protein Circular Dichroism Data Bank. *Nucleic Acids Res.* **2017,** *45* (D1), D303-D307.
3. Mavridis, L.; Janes, R. W. PDB2CD: a web-based application for the generation of circular dichroism spectra from protein atomic coordinates. *Bioinformatics* **2017,** *33* (1), 56-63.
4. Patil, R.; Mohanty, B.; Liu, B. A.; Chandrashekaran, I. R.; Headey, S. J.; Williams, M. L.; Clements, C. S.; Ilyichova, O.; Doak, B. C.; Genissel, P.; Weaver, R. J.; Vuillard, L.; Halls, M. L.; Porter, C. J. H.; Scanlon, M. J. A ligand-induced structural change in fatty acid-binding protein 1 is associated with potentiation of peroxisome proliferator-activated receptor agonists. *J. Biol. Chem.* **2019,** *294* (10), 3720-3734.
5. Sheng, N.; Li, J.; Liu, H.; Zhang, A. Q.; Dai, J. Y. Interaction of perfluoroalkyl acids with human liver fatty acid-binding protein. *Arch. Toxicol.* **2016,** *90* (1), 217-227.
6. Velkov, T.; Chuang, S.; Wielens, J.; Sakellaris, H.; Charman, W. N.; Porter, C. J. H.; Scanlon, M. J. The interaction of lipophilic drugs with intestinal fatty acid-binding protein. *J. Biol. Chem.* **2005,** *280* (18), 17769-17776.
7. Sheng, N.; Cui, R. N.; Wang, J. H.; Guo, Y.; Wang, J. S.; Dai, J. Y. Cytotoxicity of novel fluorinated alternatives to long-chain perfluoroalkyl substances to human liver cell line and their binding capacity to human liver fatty acid binding protein. *Arch. Toxicol.* **2018,** *92* (1), 359-369.
8. Yung-Chi, C.; Prusoff, W. H. Relationship between the inhibition constant (KI) and the concentration of inhibitor which causes 50 per cent inhibition (I50) of an enzymatic reaction. *Biochem. Pharmacol.* **1973,** *22* (23), 3099-3108.
9. Wolf, S. T.; Reagen, W. K. Method for the determination of perfluorinated compounds (PFCs) in water by solid-phase extraction and liquid chromatography/tandem mass spectrometry (LC/MS/MS). *Anal. Methods* **2011,** *3* (7), 1485-1493.
10. Smith, C. A.; Want, E. J.; O'Maille, G.; Abagyan, R.; Siuzdak, G. XCMS: Processing mass spectrometry data for metabolite profiling using Nonlinear peak alignment, matching, and identification. *Anal. Chem.* **2006,** *78* (3), 779-787.
11. Garcia, R. A.; Chiaia-Hernandez, A. C.; Lara-Martin, P. A.; Loos, M.; Hollender, J.; Oetjen, K.; Higgins, C. P.; Field, J. A. Suspect Screening of Hydrocarbon Surfactants in AFFFs and AFFF-Contaminated Groundwater by High-Resolution Mass Spectrometry. *Environ. Sci. Technol.* **2019,** *53* (14), 8068-8077.
12. Liu, Y. N.; Dagostino, L. A.; Qu, G. B.; Jiang, G. B.; Martin, J. W. High-resolution mass spectrometry (HRMS) methods for nontarget discovery and characterization of poly- and per-fluoroalkyl substances (PFASs) in environmental and human samples. *Trend. Anal. Chem.* **2019**.
13. Schymanski, E. L.; Jeon, J.; Gulde, R.; Fenner, K.; Ruff, M.; Singer, H. P.; Hollender, J. Identifying small molecules via high resolution mass spectrometry: communicating confidence. *Environ. Sci. Technol.* **2014,** *48* (4), 2097-2098.